

# Ultrasensitive detection of force and displacement using trapped ions

Michael J. Biercuk<sup>\*†</sup>, Hermann Uys<sup>†</sup>, Joe W. Britton, Aaron P. VanDevender and John J. Bollinger

**The ability to detect extremely small forces and nanoscale displacements is vital for disciplines such as precision spin-resonance imaging<sup>1</sup>, microscopy<sup>2</sup>, and tests of fundamental physical phenomena<sup>3–5</sup>. Current force-detection sensitivity limits have surpassed  $1 \text{ aN Hz}^{-1/2}$  (refs 6,7) through coupling of nano-mechanical resonators to a variety of physical readout systems<sup>1,7–10</sup>. Here, we demonstrate that crystals of trapped atomic ions<sup>11,12</sup> behave as nanoscale mechanical oscillators and may form the core of exquisitely sensitive force and displacement detectors. We report the detection of forces with a sensitivity of  $390 \pm 150 \text{ yN Hz}^{-1/2}$ , which is more than three orders of magnitude better than existing reports using nanofabricated devices<sup>7</sup>, and discriminate ion displacements of  $\sim 18 \text{ nm}$ . Our technique is based on the excitation of tunable normal motional modes in an ion trap<sup>13</sup> and detection through phase-coherent Doppler velocimetry<sup>14,15</sup>, and should ultimately allow force detection with a sensitivity better than  $1 \text{ yN Hz}^{-1/2}$  (ref. 16). Trapped-ion-based sensors could enable scientists to explore new regimes in materials science where augmented force, field and displacement sensitivity may be traded against reduced spatial resolution.**

Trapped atomic ions exhibit well characterized and broadly tunable (kHz to MHz) normal motional modes in their confining potential<sup>16,17</sup>. The presence of these modes, the light mass of atomic ions and the strong coupling of charged particles to external fields makes trapped ions excellent detectors of small forces with tunable spectral response<sup>13</sup>. Another advantage lies in the fact that readout is achieved through resonant-fluorescence detection using only a single laser. Previous studies have suggested that by using ions it is possible to measure forces approaching the yoctonewton scale, for instance through experiments on motional heating in Paul traps due to fluctuating electric fields<sup>18–20</sup>, or by using resonant excitation techniques<sup>17,21</sup>. In particular, small forces applied to ions in weak trapping potentials (trapping frequencies of  $\sim 0.1 \text{ MHz}$  or lower) can excite micrometre-scale motional excursions that are resolvable using real-space imaging<sup>21,22</sup>.

Although the intrinsic sensitivity of trapped ions to external forces and fields is well supported, it remains an experimental challenge to determine the maximum achievable sensitivity to a given external excitation as set by systematic limitations including the efficiency of a measurement procedure. Establishing ions as components in ultrasensitive detectors requires two primary issues to be addressed. First, a known excitation must be applied to allow precise calibration of the response of the system. Second, it must be possible to compare the results of these experiments with the existing literature on detectors based on integrated nanostructures. Our aims are to unify the seemingly disparate fields of nanotechnology and atomic devices through the use of comparable experimental conditions and a demonstration of the potential utility of ion-based sensors in nanomaterials characterization.

Our system uses a crystal of  ${}^9\text{Be}^+$  ions in a Penning trap<sup>11,12,23</sup>. Ions scatter ultraviolet laser light near  $313 \text{ nm}$ , which is almost resonant

with an internal atomic transition, cooling the ions and providing a direct imaging mechanism (see Supplementary Information for details). Scattered fluorescence is detected using an imaging system connected to a charge-coupled device (CCD) or a photomultiplier tube. In these experiments we focused on ion crystals<sup>24–26</sup> with  $n \approx 100$  ions in a two-dimensional planar array (perpendicular to the direction of the detection laser) with a diameter of  $\sim 300 \mu\text{m}$ .

In the present detection technique, known as laser Doppler velocimetry<sup>14,15</sup>, uniform ion motion at the axial centre of mass (COM) frequency (set at  $\omega_z/2\pi = 867 \text{ kHz}$  for this work), parallel to the propagation direction of the cooling laser beam, modulates the intensity of resonant fluorescence due to Doppler shifts. Under oscillatory ion motion, and with the laser detuned from resonance near the Doppler-cooling-efficiency maximum<sup>15</sup>, the intensity of ion fluorescence is modulated at  $\omega_z$ , with the amplitude approximately proportional to the motional amplitude (Fig. 1a). For uniform light collection from all ions and a detection laser power below saturation, the total detection rate of scattered photons is given by  $n\rho[1 + (2/\gamma)kz_{\text{COM}}]$ , where  $n$  is the ion number,  $\rho$  captures all hardware parameters including the quantum efficiency of the detector, the intensity of illumination and so on,  $\gamma$  is the linewidth of the atomic transition,  $k$  is the wavevector of the Doppler detection laser parallel to the ion motion, and  $\dot{z}_{\text{COM}}$  is the velocity of the axial COM coordinate.

We consider an impulse-style measurement in which a force,  $F_d \sin(\omega_d t)$ , is applied to the ions for a fixed drive time  $t_d \gg 2\pi/\omega_d$ , during which the Doppler detection laser is turned off. This means that radiation damping during excitation does not occur. We define  $F_d$  to be the amplitude of the total force applied to a crystal of  $n$  ions, and  $F_d^{(\text{ion})}$  to be the amplitude of the force applied to a single ion of mass  $m$ . After application of this drive pulse, an ion crystal with  $n$  ions will undergo a steady-state sinusoidal oscillation with velocity

$$\dot{z}_{\text{COM}}(t) = v \sin[\omega_z t + \phi] \quad (1)$$

where for  $|\omega_z - \omega_d|/\omega_z \ll 1$ , the amplitude  $v$  is given by

$$v = \frac{2F_d \omega_d}{nm(\omega_z^2 - \omega_d^2)} \sin\left[\frac{(\omega_z - \omega_d)t_d}{2}\right] \quad (2)$$

and the oscillation phase  $\phi$  is

$$\phi = \frac{(\omega_d - \omega_z)t_d}{2} \quad (3)$$

assuming no damping in a harmonic confining potential,  $m\omega_z^2 z_{\text{COM}}/2$ . Near resonance ( $\omega_z \approx \omega_d$ ), equation (2) can be written as  $v = (F_d/2nm)t_d$ .

NIST Time and Frequency Division, Boulder, Colorado, 80305, USA; <sup>†</sup>Present address: School of Physics, University of Sydney, NSW 2006, Australia (M.J.B.); Council for Scientific and Industrial Research, Pretoria, South Africa, (H.U.). \*e-mail: michael.biercuk@sydney.edu.au

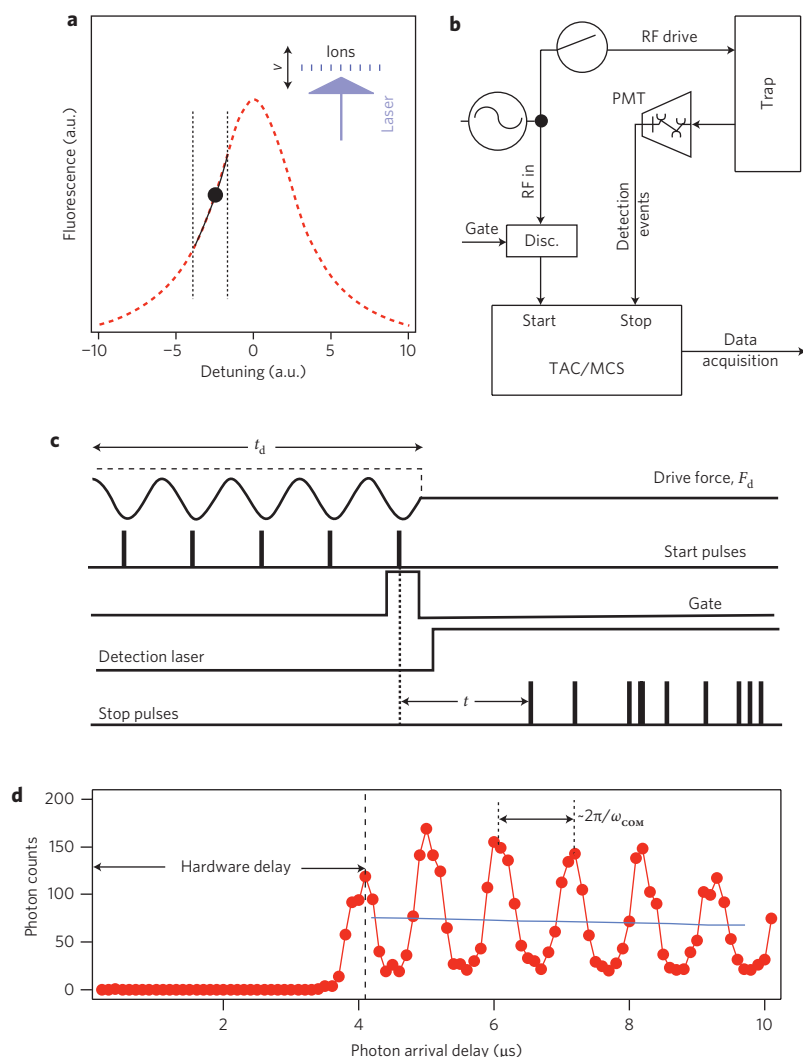


**Figure 1 | Phase-coherent Doppler velocimetry.** **a**, The dashed red line is a schematic representation of the atomic resonance used for the detection of ion motion. The  $x$ -axis is the frequency of the detection laser minus the atomic resonance frequency:  $\gamma/2\pi \approx 19$  MHz. The detection laser beam is oriented perpendicular to the plane of a two-dimensional ion crystal (see inset). An oscillating ion array periodically traces out a path on the atomic resonance profile (black line). The extent of the excursion is set by the magnitude of maximum ion velocity. Vertical dashed lines indicate the range of Doppler shifts associated with a given excursion along the resonance profile. **b**, Schematic of the Doppler detection system based on photon-arrival-time measurements. Disc., discriminator; TAC, time-to-amplitude converter; MCS, multichannel scaler; PMT, photomultiplier tube. **c**, Schematic of pulse sequencing/trigging for phase-coherent detection. This scheme is based on previous studies of micromotion nulling in a Paul trap<sup>14</sup> and studies of plasma oscillations in a Penning trap<sup>15</sup>, with the important distinction that the excitation and detection are segregated into different parts of the measurement procedure.  $F_d$  = oscillating drive force due to the a.c. electric field. The dotted line shows the pulse envelope defining the pulsed-excitation period. Start pulses synchronous with the drive are output from a discriminator and fed into the TAC or MCS. A gate pulse ensures that only the last start pulse of the excitation period triggers the TAC/MCS to begin data acquisition. The detection laser is turned on using an RF switch controlling an acousto-optic modulator, after which scattered photons may be detected. Stop pulses are generated by the detection of scattered photons using the PMT and are fed to the TAC/MCS. **d**, Histogram of photon arrival times relative to start pulses generated synchronously with an RF drive of the COM mode on resonance. The horizontal axis corresponds to the time delay  $t$  indicated in **c**. Photon arrivals are bunched with a periodicity given by the driven COM oscillation period, following hardware delays. The solid blue line is an exponential fit to the data used to remove a background scattering rate (see Supplementary Information).

Ion motion induced by the application of this driving force will be superimposed on a noisy background due to the finite temperature of the axial mode and stray electric fields. The ability to discern a small oscillating signal of known frequency in the presence of a large background has been well established through use of phase-sensitive detection<sup>27</sup>. In these techniques, which have been shown to be applicable in almost any setting, a signal of interest is discriminated by synchronization of the response of a target system to a master oscillator that produces or modulates the excitation. Broadband environmental noise is consequently excluded, and only the integrated noise over the narrow bandwidth of the measurement is germane.

The temporal modulation of ion fluorescence due to the applied drive is detected phase-coherently by recording scattered-photon arrival times using a photomultiplier tube relative to a trigger synchronized to the external drive force. Photon arrival times relative to the drive force are then determined using a time-to-amplitude converter (TAC) or multichannel scaler over  $N$  iterations of the experiment. Any noise, however, is not phased with the drive, and averaging  $N$  times increases the contrast of the desired signal relative to the background noise by a factor of  $N^{1/2}$ .

Precise characterization of the achievable force- and displacement-detection sensitivity requires the application of a

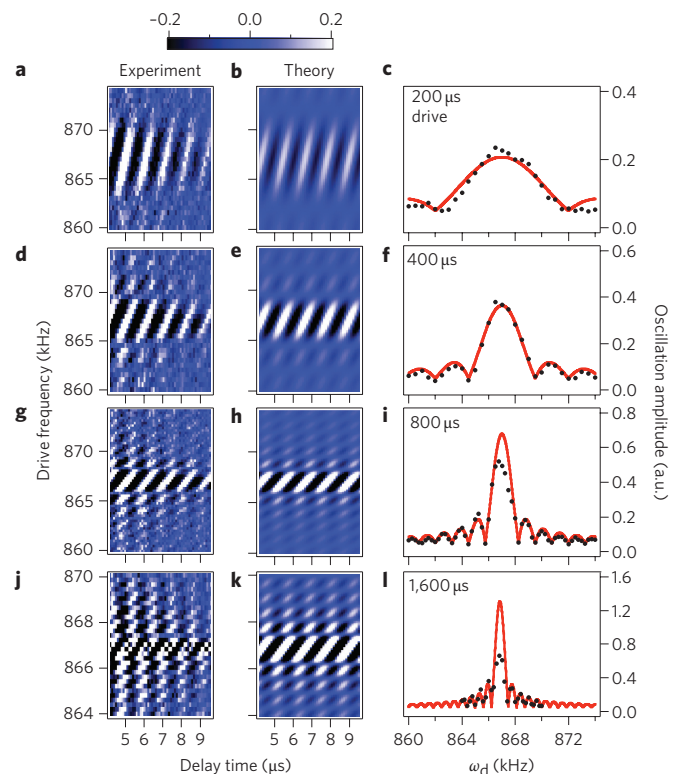
well-calibrated drive force. Such a force is generated using the electric field from a radiofrequency (RF) voltage applied to an endcap electrode on the trap, in a similar manner to the resonant electric-field excitation techniques used in cantilever experiments<sup>28</sup> (Fig. 1b,c). The electric field at the location of the ions is calibrated using a measurement of the static deflection of a planar ion crystal by sideview imaging under application of a static voltage to the same endcap electrode (see Supplementary Information). As an example, for an applied zero-to-peak voltage of  $165 \pm 10 \mu\text{V}$  (nominal RF power,  $P_{\text{RF}} = -70 \text{ dBm}$ ), we determined an electric field of  $1.8 \pm 0.1 \text{ mV m}^{-1}$  at the location of the ions, and a corresponding force  $F_0^{(\text{ion})} = 290 \pm 18 \text{ yN}$  per ion.

Figure 1d shows a typical histogram of the arrival times of the first detected photon synchronized to the drive for  $\omega_d = \omega_z$ . For short times, no photons are detected due to hardware delays (mainly because of the response of the acousto-optic modulator (AOM) switch). Once photon-detection events begin accumulating after  $\sim 4 \mu\text{s}$ , we find a bunching of photon arrival times with a period commensurate with the  $1.15\text{-}\mu\text{s}$  period of the COM oscillation. Phase information is captured in the absolute locations of the histogram maxima along the time axis. This approach allows the target system to have a variable shot-to-shot phase difference from the master oscillator as experimental parameters are swept, thus providing more information than standard lock-in detection, in which the detection phase offset is fixed.

We studied the Doppler velocimetry signal as a function of  $\omega_d$  and  $t_d$ . The measurement scans the drive frequency and records a histogram of stop-pulse delays relative to the drive-force trigger (the start pulse). Modulation of the scattered photon rate is plotted as a colourscale, after correcting for an exponential decay factor due to the triggering technique (see Supplementary Information). The first column of Fig. 2 (a,d,g,j) shows experimental measurements of COM-mode excitation, and the second column (b,e,h,k) shows theoretical calculations based on the formulae above. In these calculations,  $t_d$  and  $\omega_z$  are fixed, with a variable drive strength and background, both of which are held the same for all  $t_d$ .

The theoretical calculations match well with the experimental data, replicating both qualitative and quantitative features. Doppler velocimetry indicates a linear phase shift in the oscillator as  $\omega_d$  is tuned through resonance, and the excitation of the oscillator is zero when  $|\omega_d - \omega_z| = 2\pi/t_d$ , such that during the driving period the external force and system response desynchronize and resynchronize<sup>29</sup>. Moreover, in addition to the central resonance feature, oscillation sidelobes appear, separated by the detuning period  $2\pi/t_d$ , and we have seen ten sidelobes for strong RF excitation. In the experimental data, a damping of the oscillation strength is also observed as a function of the delay time due to radiation pressure from the detection laser. This effect is not accounted for in the calculations shown in the second column of Fig. 2.

The linewidth of the resonance scales as the inverse of  $t_d$  (Fig. 2c,f,i,l). Here we plot the oscillation amplitude (using the standard deviation of the photon-arrival-time histogram for all  $t$  as a proxy) as a function of  $\omega_d$ , and find that the amplitude of the measured ion velocity matches well with theoretical predictions over all  $\omega_d$ . The quality factor of the COM mode is limited by the presence of dark ions produced by background gas collisions and by power-supply instabilities, but is high relative to the Fourier-limited linewidth of  $\omega_z$  for the values of  $t_d$  shown here. Agreement between data and theory breaks down for the largest values of  $t_d$ , which induce the largest ion velocities. Under these conditions, the ions are driven out of the linear-response regime of Doppler velocimetry, or even to the blue side of the resonance, resulting in reduced scatter rates that manifest as dips in the central oscillation lobe (Fig. 2j,l). Reducing the RF excitation removes these effects. The nonlinear velocimetry response can also be used as an independent calibration of the applied force (by means of equation (2) near resonance), agreeing to within a factor of



**Figure 2 | Phase-coherent detection of the COM mode by RF excitation, where  $F_d^{(\text{ion})} = F_0^{(\text{ion})}$ .** **a,b,d,e,g,h,j,k**, Residual of fit to exponential decay in photon arrival times for four driving-pulse durations, expressed as a colourscale for experiment (**a,d,g,j**) and theory (**b,e,h,k**). The horizontal axis represents the arrival delay from the start pulse; the vertical axis represents drive frequency. The amplitude of the oscillations decays with delay time due to radiation damping from the detection laser and is not accounted for in the theoretical plots. **c,f,i,l**, Standard deviation of photon arrival times as a function of drive frequency. Each data point represents the standard deviation of a horizontal slice of the two-dimensional plots (left) and illustrates resonant excitation of the COM mode as in Fig. 1c (standard deviation over the whole measurement period is used as a proxy for oscillation amplitude). The solid lines represent theoretical fits using fixed drive times with the force strength and a constant offset used as free parameters. Each row of plots in the figure corresponds to a fixed drive time. Fit parameters extracted from a 200- $\mu\text{s}$  drive duration were used for longer drive periods. Breakdown in fit quality on resonance increases with drive time, because strong excitation causes the ions to be shifted out of the linear response regime to the blue side of the Doppler resonance, hence decreasing fluorescence.

order unity with the electric-field calibration described above (see Supplementary Information).

The force detection sensitivity was analysed by systematically reducing the excitation strength and examining the system response through Fourier analysis. Figure 3a shows a one-dimensional slice of the time-domain Doppler velocimetry signal for diminishing values of  $F_d$ , accomplished by reducing  $P_{\text{RF}}$  ( $t_d$  is fixed at 1 ms) using a planar array of  $n = 130 \pm 10$  ions. To minimize the number of required experimental cycles we used a multichannel scaler and collected more than one photon ( $\sim 3\text{--}5$ ) per experimental cycle.  $F_d^{(\text{ion})}$  was varied from  $F_0^{(\text{ion})}$  to  $F_0^{(\text{ion})}/100$ , and the magnitude of the system response reduced commensurately. These data were Fourier transformed (omitting the systematic delay for short times) and the results displayed on a semi-logarithmic plot in Fig. 3b, demonstrating a spectral peak near the COM resonance frequency with diminishing signal-to-noise ratio (SNR).

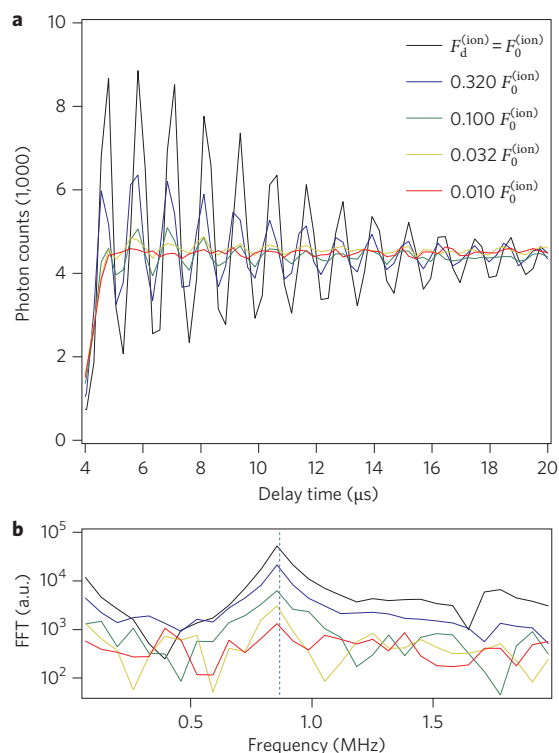


**Figure 3 | Calibration of force-detection sensitivity by Fourier analysis.** **a**, Temporal response to applied  $F_d^{(tot)} = nF_d^{(ion)}$  with  $n = 130$  for decreasing drive strength and  $t_d = 1$  ms. Total experiment time  $\tau_M$  is  $\sim 56$  s for each trace, including all measurement and dead time (recoiling, photon detection, hardware delays), corresponding to  $\sim 40,000$  excitation/detection cycles. The observed decay of oscillation magnitude is due to radiation damping occurring once the detection laser is turned on. **b**, FFT of temporal response traces recorded in **a**, plotted on a semi-logarithmic scale, with the same colour coding as in **a**. A spectral peak is apparent at  $\omega_{COM}$ , which diminishes in strength with decreasing  $F_d^{(tot)}$ . The spectral peak has  $SNR \approx 2.3$  for  $F_d^{(ion)} = 0.010 F_0^{(ion)}$  (see text).

With  $F_d^{(ion)} \equiv F_0^{(ion)}/100 = 2.9 \pm 0.18$  yN/ion and  $n = 130 \pm 10$ , the total force on the array was  $F_d = 377 \pm 37$  yN. From the spectral peak at  $\omega_z$  we calculated the SNR (here 2.3) and accounted for the measurement bandwidth to extract a force-detection sensitivity of  $\sim 1,200$  yN Hz $^{-1/2}$  for SNR = 1 (see Supplementary Information).

The COM axial amplitude of an excitation may be expressed as

$$z_{COM} = \frac{F_d t_d}{2nm_{Be}\omega_z} \quad (4)$$

Sensitivity to spatial displacement may be characterized by considering small values of both  $F_d$  and  $t_d$ . For an excitation (as above) with  $t_d = 1$  ms,  $F_d = 377$  yN and  $n = 130$ , it is possible to discriminate spatial displacements of  $z_{COM} \approx 18$  nm (sensitivity  $\approx 58$  nm Hz $^{-1/2}$ ). This amplitude is comparable to the thermal axial extent of the COM mode for a crystal of 130 ions (11 nm for  $T = 0.5$  mK), and an order of magnitude less than the thermal axial extent of an individual ion in the array (120 nm). These absolute and relative sizes indicate that real-space imaging of ion excitation is not possible using, for example, a CCD camera. An excitation of this magnitude is also comparable to common values associated with nanomechanical resonators.

Characterization of the minimum achievable force-detection sensitivity was accomplished by producing a large motional response to a given applied force. For a given  $F_d^{(ion)}$ , the Doppler

velocimetry signal near resonance grows linearly with  $t_d$ , but detection sensitivity only increases (gets worse) as  $t_d^{1/2}$ . We have confirmed this scaling using ion crystals with  $n = 60, 130$  and  $530$  ions, observing an approximately linear increase in measured SNR up to  $t_d = 10$  ms (without bandwidth normalization). For larger values of  $t_d$ , the experimental drifts of  $\omega_z$  on timescales comparable to the data acquisition time become significant relative to the narrowed Fourier response of the driven oscillator.

The smallest force we detected was  $\sim 170$  yN, using a crystal of  $n = 60 \pm 5$  ions and  $t_d = 10$  ms, as described above. Averaging over data acquired with different values of  $F_d$  (normalizing by the SNR for different values of  $F_d$  should yield similar values of force detection sensitivity), we found a minimum force-detection sensitivity of  $390 \pm 150$  yN Hz $^{-1/2}$ . The experimental uncertainty includes statistical fluctuations in averaging, uncertainty in the ion number, uncertainty in the calibration of the applied electric field, and imprecision in the calculation of the SNR. Improvement in this value relative to that extracted from Fig. 3b may be derived from both the increased drive time and the reduced ion number (see Supplementary Information).

It is important to distinguish between the measured systemic detection sensitivity (force or displacement) and the intrinsic sensitivity of the ions. The ions respond to the external stimulus in a bandwidth set by  $t_d^{-1}$ , for these experiments  $>3,000$  times wider than  $\tau_M^{-1}$ , where  $\tau_M$  is the measurement time. Thus, the intrinsic ion sensitivity is at least 50 times better than reported in our measurement, and in line with sensitivities that may be derived from heating rate measurements $^{18-20}$ . However, in any experiment it is necessary to extract information from the system and account for inefficiencies in the readout technique when calculating the sensitivity of the system.

Considerable systematic improvement is possible before the present system becomes limited by the intrinsic sensitivity of trapped ions to forces and fields. Realistic experimental improvements may be achieved by increasing the measurement bandwidth, primarily through improved light-collection efficiency (measurements are currently shot-noise limited). For instance, experimental modifications allowing for large-solid-angle light collection and sampling during measurement at the Nyquist limit both reduce the required number of experimental cycles,  $N$ , and hence  $\tau_M$ . Such improvements could allow the realization of a force-detection sensitivity  $\sim 1.7$  yN Hz $^{-1/2}$ , which is comparable to previously published calculations $^{16}$  (see Supplementary Information). Additionally, systematic improvements that increase the stability of  $\omega_z$  will permit longer drive times and hence improved force-detection sensitivities; our system is currently limited by the effects of background gas collisions and power-supply instabilities.

This technique has been successfully applied for the detection of optical dipole forces induced by Raman lasers. Additionally, the Penning trap permits experiments using values of  $n$  well over  $1 \times 10^6$ , thus allowing optimization of sensitivity to electric fields (large total charge desirable) rather than applied forces (small total mass desirable). Given a crystal of this size and similar experimental conditions, we could likely achieve an electric field sensitivity of  $\sim 500$  nV m $^{-1}$  Hz $^{-1/2}$ , with intrinsic sensitivity limits still lower.

The presented experiments have demonstrated phase-coherent excitation and detection of yN-level forces and nm-scale displacements induced by oscillating electric fields using trapped ions. Our measurements have validated published calculations $^{16}$  suggesting that force-detection sensitivities of  $\sim 1$  yN Hz $^{-1/2}$  are possible for single ion experiments, due to the light mass of harmonically bound trapped ions and the presence of a strong readout technique. Essentially, we have included in our detection-sensitivity measurements all relevant readout times, experimental dead times, hardware delays and the like, making this a very conservative estimate of achievable force-detection sensitivity.

Beyond simply measuring extremely small forces, this detection technique provides the facility to discriminate motional excitations more than an order of magnitude smaller than the thermal extent of a single ion, and deep below the resolution limits imposed by typical imaging systems. Because the size of the motional excursion of an ion scales as  $\omega_z^{-1}$ , for forces of the magnitude detected here it is difficult to directly image motional excitations at frequencies larger than  $\sim 0.1$  MHz. Thus, phase-sensitive detection of ion motion may enable high-frequency measurements as a part of a tunable, broadband detector.

One potential shortcoming of this detection mechanism relates to the use of a phase-synchronous protocol. In circumstances such as detector calibration or the application of an optical dipole force, it is straightforward to synchronize detection events to the externally applied force. In general the problem becomes significantly more complicated when trying to measure an unknown force. However, it is typically possible to modulate an unknown external signal near  $\omega_z$  in such a way as to permit synchronization of detection events<sup>24</sup>. For instance, in surface science or field mapping studies such as proposed in ref 16, a drive signal in the target device (such as a current bias) could be modulated directly, producing a time-varying, detectable force or field. Synchronization with the modulation envelope signal would then permit a performance similar to that achieved in our experiments. In such an approach the use of an ion-based detector could provide a means to map forces and fields at target–probe distances not generally accessible using cantilevers or other comparable approaches. As an additional example, in studying the dynamics of surface charge accumulation, a laser producing photo-excited charge could be modulated to provide a synchronization signal<sup>30</sup>. Doing so, and then using phase-synchronous detection, would permit the study of high-frequency charging dynamics that are not accessible in standard ‘time-integrated’ detection techniques.

The results presented here build on a strong foundation laid by previous trapped-ion experiments, and suggest that ion-based sensors may form a vital tool for sensitive measurements in nanoscale science. Their utility will be maximized in applications where lateral spatial resolution may be traded against increased overall sensitivity and the ability to detect forces and fields with standoff distances greater than achievable using detectors based on integrated nanodevices. Realistic, field-deployable sensors will probably require the use of integrated ion-trap chips with asymmetric potentials for directional force detection and three-dimensional spatial mapping. It may also be desirable to use sub-Doppler cooling and sideband-detection mechanisms<sup>17,18</sup> for the measurement of stochastic fields and forces.

Received 8 June 2010; accepted 14 July 2010;

published online 22 August 2010

## References

- Rugar, D., Budakian, R., Mamin, H. J. & Chui, B. W. Single spin detection by magnetic resonance force microscopy. *Nature* **430**, 329–332 (2004).
- Binnig, C., Quate, C. F. & Gerber, C. Atomic force microscope. *Phys. Rev. Lett.* **56**, 930–933 (1986).
- Mohideen, U. & Roy, A. Precision measurement of the casimir force from 0.1 to 0.9  $\mu\text{m}$ . *Appl. Phys. Lett.* **81**, 4549–4552 (1998).
- Volokitin, A. I. & Persson, B. N. J. Theory of friction: the contribution from a fluctuating electric field. *J. Phys. Condens. Matter* **11**, 345–359 (1999).
- Arkani-Hamed, N., Dimopoulos, S. & Dvali, G. The hierarchy problem and new dimensions at a millimeter. *Phys. Lett. B* **429**, 263–272 (1998).
- Mamin, H. J. & Rugar, D. Sub-attoneutron force detection at millikelvin temperatures. *Appl. Phys. Lett.* **79**, 3358–3360 (2001).
- Teufel, J. D., Donner, T., Castellanos-Beltran, M. A., Harlow, J. W. & Lehnert, K. W. Nanomechanical motion measured with an imprecision below that at the standard quantum limit. *Nature Nanotech.* **4**, 820–823 (2009).

- Knobel, R. G. & Cleland, A. N. Nanometer-scale displacement sensing using a single-electron transistor. *Nature* **424**, 291–293 (2003).
- Lahaye, M. D., Buu, O., Camarota, B. & Schwab, K. C. Approaching the quantum limit of a nanomechanical resonator. *Science* **304**, 74–77 (2004).
- Regal, C. A., Teufel, J. D. & Lehnert, K. W. Measuring nanomechanical motion with a microwave cavity interferometer. *Nature Phys.* **4**, 555–560 (2008).
- Brewer, L. R. *et al.* Static properties of a non-neutral  $^9\text{Be}^+$  ion plasma. *Phys. Rev. A* **38**, 859–873 (1988).
- Biercuk, M. J. *et al.* High-fidelity quantum control using ion crystals in a penning trap. *Quantum Inf. Comput.* **9**, 920–949 (2009).
- Heinzen, D. J. & Wineland, D. J. Quantum-limited cooling and detection of radio-frequency oscillations by laser-cooled ions. *Phys. Rev. A* **42**, 2977–2994 (1990).
- Berkeland, D. J., Miller, J. D., Bergquist, J. C., Itano, W. M. & Wineland, D. J. Minimization of ion micromotion in a Paul trap. *J. Appl. Phys.* **83**, 5025–5033 (1998).
- Mitchell, T. B., Bollinger, J. J., Huang, X.-P. & Itano, W. M. Doppler imaging of plasma modes in a penning trap. *Opt. Express* **2**, 314 (1998).
- Maiwald, R. *et al.* Stylus ion trap for enhanced access and sensing. *Nature Phys.* **5**, 551–554 (2009).
- Wineland, D. J. *et al.* Experimental issues in coherent quantum-state manipulation of trapped atomic ions. *J. Res. NIST* **103**, 259–328 (1998).
- Turchette, Q. A. *et al.* Heating of trapped ions from the ground state. *Phys. Rev. A* **61**, 063418 (2000).
- Deslauriers, L. *et al.* Zero-point cooling and low heating of trapped  $^{111}\text{Cd}^+$  ions. *Phys. Rev. A* **70**, 043408 (2004).
- Labaziewicz, J. *et al.* Temperature dependence of electric field noise above gold surfaces. *Phys. Rev. Lett.* **101**, 180602 (2008).
- Drewsen, M., Mortensen, A., Martinussen, R., Staunum, P. & Sorensen, J. L. Nondestructive identification of cold and extremely localized single molecular ions. *Phys. Rev. Lett.* **93**, 243201 (2004).
- Staunum, P. F., Højbjerg, K. & Drewsen, M. Sympathetically-cooled single ion mass spectrometry, in *Practical aspects of trapped ion mass spectrometry* (eds March, R. E. & Todd, J.F.J.) (CRC Press, 2010).
- Major, F. G., Gheorghie, V. N. & Werthe, G. *Charged Particle Traps: Springer Series on Atomic, Optical, and Plasma Physics* (Springer, 2005).
- Mitchell, T. B. *et al.* Direct observations of structural phase transitions in planar crystallized ion plasmas. *Science* **282**, 1290–1293 (1998).
- Huang, X.-P., Bollinger, J. J., Mitchell, T. B. & Itano, W. M. Phase-locked rotation of crystallized non-neutral plasmas by rotating electric fields. *Phys. Rev. Lett.* **80**, 73–76 (1998).
- Jensen, M. J., Hasegawa, T., Bollinger, J. J. & Dubin, D. H. E. Rapid heating of a strongly coupled plasma near the solid–liquid phase transition. *Phys. Rev. Lett.* **94**, 025001 (2005).
- Horowitz, P. & Hill, W. *The Art of Electronics* (Cambridge Univ. Press, 2006).
- Stowe, T. *et al.* Attonewton force detection using ultrathin silicon cantilevers. *Appl. Phys. Lett.* **71**, 288–290 (1997).
- Leibfried, D. *et al.* Experimental demonstration of a robust high-fidelity geometric two ion-qubit phase gate. *Nature* **422**, 412–415 (2003).
- Harlander, M., Brownutt, M., Hansel, W. & Blatt, R. Trapped-ion probing of light-induced charging effects on dielectrics. Preprint at <http://arXiv.org/abs/1004.4842> (2010).

## Acknowledgements

The authors thank K. Lehnert, D. Leibfried, D.J. Reilly, T. Rosenband and D.J. Wineland for useful discussions. Thanks also go to J. Kitching and U. Warring for their comments on the manuscript. The authors acknowledge research funding from the Defense Advanced Research Projects Agency (DARPA), the DARPA Optical Lattice Emulator program, and the National Institute of Standards and Technology (NIST) Quantum Information Program. M.J.B. acknowledges fellowship support from the Intelligence Advanced Research Projects Activity and Georgia Tech. H.U. acknowledges support from the Council for Scientific and Industrial Relations, South Africa. This manuscript is a contribution of NIST and not subject to US copyright.

## Author contributions

M.J.B., H.U. and J.J.B. conceived, designed and performed the experiments and co-wrote the manuscript. J.W.B. contributed to experimental measurements and data analysis. A.P.V.D. assisted with optics hardware and the hardware–software interface.

## Additional information

The authors declare no competing financial interests. Supplementary information accompanies this paper at [www.nature.com/naturenanotechnology](http://www.nature.com/naturenanotechnology). Reprints and permission information is available online at <http://npg.nature.com/reprintsandpermissions/>. Correspondence and requests for materials should be addressed to M.J.B.